Catalysis Today 165 (2011) 160–170

Contents lists available at ScienceDirect

Catalysis Today

journal homepage: www.elsevier.com/locate/cattod

Electrocatalyst design from first principles: A hydrogen-production catalyst inspired by nature

Federico Zipoli[a], Roberto Car[a,b], Morrel H. Cohen[a,c], Annabella Selloni[a,*]

[a] Department of Chemistry, Princeton University, Washington Road, Princeton, NJ 08544, United States
[b] Princeton Institute for the Science and Technology of Materials, Princeton University, Princeton, NJ 08544, United States
[c] Department of Physics and Astronomy, Rutgers University, Piscataway, NJ, 08854, United States

ARTICLE INFO

Article history:
Received 20 August 2010
Received in revised form 7 December 2010
Accepted 8 December 2010
Available online 15 January 2011

Keywords:
Electrocatalysis
Hydrogen production
First principles molecular dynamics

ABSTRACT

Sustainable economic production of hydrogen from water and sunlight is an attractive goal. It requires an active electrocatalyst comprised of earth-abundant elements. Such a catalyst exists in nature, the $[FeFe]_H$ cluster in the active site of the di-iron hydrogenase enzymes. To reach the required specific activity within an actual solar hydrogen-production system, the catalytically active site must, figuratively, be stripped from the enzyme, attached to a cathode or photocathode, and immersed in water. Thus modifications of the composition and structure of the cluster are to be found which allow for stable attachment to the electrode surface and for maintenance of its integrity and activity throughout the H_2-producing cycle in an environment drastically different from that in the enzyme. We have addressed that problem by simulating the behavior of model clusters by first-principles electronic-structure and molecular-dynamics simulations. We review our studies, first of the $[FeFe]_H$ cluster in vacuum; next of the $[FeFe]_H$ cluster in water; then of a systematic sequence of modifications which culminates with the design of the successful phosphorous-substituted $[FeFe]_P$ cluster; and, finally, an investigation of the H_2 producing cycle of $[FeFe]_P$. We then discuss the limitations of our results and conclude with a brief consideration of future directions.

1. Introduction

Sustainable economic production of hydrogen from water and sunlight is an attractive goal. The hydrogen would serve as a useful store of solar energy. The resources from which it would be produced, water and sunlight, are obviously sustainable, the water providing the protons and the sunlight the electrons for the hydrogen evolution reaction $2H^+ + 2e^- \rightarrow H_2$. Producing the hydrogen economically via that reaction on the required scale requires an active electrocatalyst comprised of earth-abundant elements. Such a catalyst exists in nature, the $[FeFe]_H$ cluster in the active site of the di-iron hydrogenase enzymes of hydrogen-producing bacteria. Under optimum conditions, each molecule of the *DesulfoVibrio desulfuricans* enzyme can produce 9000 molecules of hydrogen per second at room temperature [1]. However, the enzyme itself is so large that to reach the required specific activity within an actual hydrogen-production system [2], the catalytically active site must, figuratively, be stripped from the enzyme, attached to a cathode or photocathode, and immersed in water. That poses a challenging problem: *Modifications of the composition and structure of the cluster are to be found which allow for stable attachment to the electrode surface and maintenance of its integrity and activity throughout the H_2-producing cycle in an environment drastically different from that in the enzyme.* We have addressed this problem as one in theoretical catalyst design with the intent of providing guidance for the actual synthesis of a functionalized electrode and ultimately the fabrication of a hydrogen-production system. We review here the encouraging results we have obtained thus far and summarize the remaining tasks.

The theoretical methods available for consideration are (1) molecular dynamics (MD) using empirical force fields to simulate nuclear motion without addressing changes in the electronic structure, (2) QM/MM which treats the electrons of that part of the system centrally involved in the chemical reactions quantum mechanically and the rest by MD, and (3) full first-principles quantum-mechanical treatment of all of the electrons in the system (FPMD). In FPMD, the force fields that determine the nuclear motion do not require empirical fitting but are generated on the fly from the quantum-mechanical ground state of the electrons. MD cannot be used as it cannot capture the dynamics of the electron transfers central to hydrogen production as well as other significant changes of electron structure during the production cycle. As the system to be studied is quite large, comprised of the electrode, the catalytic cluster functionalizing the electrode surface, and the water

* Corresponding author.
E-mail address: aselloni@princeton.edu (A. Selloni).

0920-5861/$ – see front matter © 2010 Elsevier B.V. All rights reserved.
doi:10.1016/j.cattod.2010.12.030

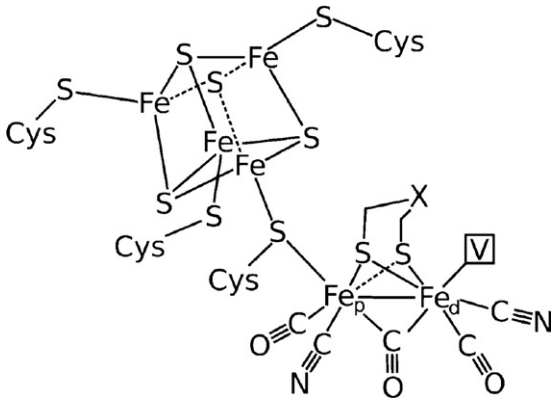

Fig. 1. Sketch of the active site of the di-iron hydrogenases. It is composed of the catalytically active $[FeFe]_H$ cluster, connected to an Fe_4S_4 cubane through the sulfur of a cysteine (Cys) in the enzyme's backbone. The distal iron (Fe_d) of $[FeFe]_H$ has a vacant site, indicated by V. The X in the chelating S–CH_2–X–CH_2–S group stands for CH_2, NH or O [4].

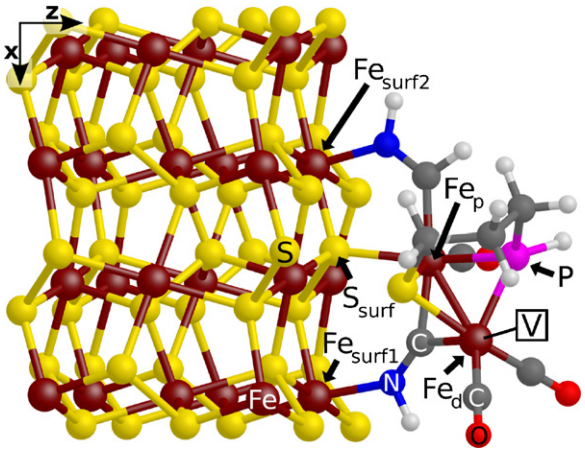

Fig. 2. Side view of the $[FeFe]_P$ cluster linked to an S-atom (S_{surf}) on the FeS_2 (1 0 0) surface via a direct Fe_p–S_{surf} bond. The distal and the proximal irons are indicated by the labels Fe_d and Fe_p, respectively. Fe_p and Fe_d are bridged by an S–CH_2–CH_2–CH_2–P group. A $(CNH)_d$ group bridges the Fe_p and Fe_d and is connected to an Fe-atom of the surface (Fe_{surf1}) via a dative bond between its N and Fe_{surf1}. The distal iron has a vacant site, indicated by V. A second dative bond forms between a second surface iron (Fe_{surf2}) and the N atom of $(CHNH)_p$. Fe atoms are dark red; S atoms are yellow; the P atom is pink; C atoms are dark gray; N atoms are blue; O atoms are red; and H atoms are shaded. (For interpretation of the references to color in this figure legend, the reader is referred to the web version of the article.)

in which the functionalized electrode is immersed, one might think that QM/MM would be the method of choice for reducing computational costs. However, that part of the system which must be treated quantum-mechanically is sufficiently large that QM/MM offers little advantage over FPMD with regard to reducing computational costs and introduces errors through its treatment of the transition region between the quantum and classical domains. Accordingly, in our efforts to solve the design problem, we have used electronic structure methods and FPMD for the entire system, as illustrated in Section 2.

In the $[FeFe]_H$ cluster two iron atoms are coordinated with CO and CN ligands and bridged by a chelating group, S–CH_2–X–CH_2–S, where X can be an NH (DTMA) or CH_2 (PDT) group, cf. Fig. 1 [3]. In the enzyme one of the two iron atoms, the proximal iron (Fe_p), is connected to an iron–sulfur Fe_4S_4 cluster (a cubane) via the *sulfur* of a cysteine, Fig. 1 [3]. The other iron in the $[FeFe]_H$ cluster is the distal iron (Fe_d). In the cluster configuration corresponding to the enzyme's active ready state [4], the μ-CO configuration in Fig. 1, there is one CO, the μ-CO, bridging the two iron atoms, leaving a vacant coordination site, V, on Fe_d. Hydrogen production occurs at V. Each of the sulfurs of the chelating group is linked to each of the irons. The (1 0 0) surface of pyrite, FeS_2, has a similar configuration of iron and sulfur atoms, suggesting that the cluster could be stably linked to that surface. Moreover, FeS_2 is a semiconductor with a band gap of ∼0.9 eV [5], making it suitable for incorporation into a multi-junction photovoltaic device for generating electrons efficiently from sunlight. Accordingly, we have chosen pyrite as the electrode in our design and have simulated the functionalization of its (1 0 0) surface.

The full system of electrode, attached catalyst, and neutral or acidified water is physically and chemically complex. Searching for an effective design by first-principles simulation is consequently computationally complex. We adopted a stepwise strategy to deal with that complexity. We started by studying the $[FeFe]_H$ cluster in vacuo [6], added water [7], attached it to the electrode and systematically changed the structure and composition of the cluster to achieve stable linkage to the electrode and structural integrity throughout a cycle of facile hydrogen production [8], and studied in detail the H_2-producing cycle of the resulting modified cluster, $[FeFe]_P$, linked to the electrode as shown in Fig. 2 [9]. [We use the symbol $[FeFe]_P$ to represent either the cluster or the functionalized electrode depending on context.] There were many essential lessons learned along the way without which it would have been hopelessly impractical to have attempted a *de novo* attack on the complete system.

In the following, we briefly describe our vacuum studies of the naked active site in Section 3, our studies of the influence of a water environment on the active site in Section 4, and the design and functioning of the successful electrode-catalyst complex in Section 5. We discuss the limitations of our results and what can be done to mitigate them in Section 6. We conclude in Section 7 with a status report and consider future directions.

2. Methods

Our studies have been based on Car–Parrinello [10] FPMD simulations of the $[FeFe]_H$ cluster and of the functionalized electrode in vacuo and in a liquid–water environment with or without hydronium ions. The FPMD simulations were performed within the framework of density-functional theory in the local-spin-density approximation supplemented by generalized-gradient corrections [11] as implemented in the CP code of the Quantum ESPRESSO package [12]. In all our work, the systems were modeled with periodic boundary conditions imposed on a cubic or tetragonal simulation cell with its lattice parameters chosen as appropriate in each case. To illustrate our methods, the following paragraph gives specifics for the systems studied in reference [8] in which the design process leading to the $[FeFe]_P$ cluster is described, cf. Section 5.1 below.

We employed ultrasoft pseudopotentials [13,14] with plane-wave expansions of the Kohn–Sham orbitals and of the augmented density up to kinetic-energy cutoffs of 30 Ry and 240 Ry, respectively. The pyrite electrode was modeled in a slab geometry with (1 0 0) surfaces and 3D periodic boundary conditions at the experimental lattice constant, 5.428 Å [15]. (Our theoretical lattice constant, computed with fully converged Brillouin zone (BZ) sampling, is 5.404 Å, only 0.4% shorter than the experimental one.) We used a 2×2 supercell having the ideal bulk termination of the slab. The slab was nine atomic layers thick (24 FeS_2 units, cf. Fig. 2) in a tetragonal simulation box with $a = 10.856$ Å, $c = 21.712$ Å, and a vacuum width between slabs of 15 Å. The atoms of the three bottom layers were fixed to their positions in the clean surface during geometric optimizations of the supported catalyst, whereas all atoms were free to move during the FPMD simulations. We used only the Γ point to sample the surface BZ for both FPMD and structural opti-

mizations. Test calculations comparing the results of the Γ-point integration with those of a k-point mesh showed differences in relative energies of the order of k_BT. We attached a sequence of progressively further modified di-iron $[FeFe]_H$ clusters (see Section 5.1) to the FeS_2 (1 0 0) surface and added 37 water molecules between slabs to simulate immersion of the supported cluster in water of real density. A fictitious electronic mass of 350 au and a time step of 0.072 fs were used in the FPMD simulations. The deuterium mass was used for hydrogen to allow for a longer time step. Constant temperature was imposed on the ions by a Nosé-Hoover thermostat [16,17]. In situations where the system's HOMO–LUMO energy gap was "small" (less than 0.1 eV), adiabaticity of the FPMD trajectory was maintained by coupling two separate Nosé-Hoover thermostats to the nuclear and electronic subsystems [18]. Static calculations on the isolated $[FeFe]_H$ cluster in vacuo were performed using the PW code of the Quantum ESPRESSO package [12]. Energy barriers were calculated using the climbing-image nudged-elastic-band (NEB) [19] and string methods [20]. For geometry optimizations and energy-barrier determinations, the norm of the force vector was required to be smaller than 5 meV/Å at convergence. Different pseudopotentials were used for the iron atoms of the cluster and for those of the pyrite slab, with 16 and 8 electrons explicitly treated as valence electrons, respectively. We verified that this choice reduced the computational cost without affecting the accuracy of our description of the delicate chemistry involving the two iron atoms of the $[FeFe]_H$ or $[FeFe]_P$ cluster. The validity of DFT for addressing the electronic and chemical properties of the FeS_2 surface [21–24] and the di-iron cluster in different environments [6,7,25–34] is well established. Because the duration of our simulations is limited to a few picoseconds, each computed trajectory may remain sensitive to the initial condition imposed. To overcome this possible source of bias, we normally computed several trajectories spanning a representative range of initial conditions.

The choices we made of the density functionals, the pseudopotentials, and the simulation cell parameters are aimed at achieving a satisfactory compromise between computational cost and accuracy, a compromise which imposes limitations on the accuracy of our results. For example, the rate limiting step in H_2 production by the $[FeFe]_P$ cluster turns out to be its first protonation, for which we found an upper bound for the free-energy barrier of 8.2 kcal/mol (0.36 eV) [9]. This value is sensitive to the choices of the density functional and cell parameters, and especially to the accuracy of the thermodynamic integration method we used to calculate it, as discussed further in Section 6.

3. The naked active site

In addition to experimental studies of the enzyme [35–42], there have been many theoretical studies of the isolated $[FeFe]_H$ cluster in vacuo primarily focused on understanding how it works within the enzyme [25–28,30–34,43–46]. Instead, our focus has been on building a basis for the design of an electrocatalyst active in water. To extract the cluster from the enzyme, the bonds tying it to the cubane must be cut, figuratively speaking. As commonly done in prior work by others [26,27], we have simply replaced the cysteine linked to the cubane by a methylthiol, as shown in Fig. 3a for the μ-CO configuration found in the enzyme. To maintain resemblance to the enzyme, we chose the chelating chain to be DTMA, with its group X being NH, consistent with recent HYSCORE observation of the hyperfine structures of three distinct N nuclei in the active site of the enzyme [47]. We then placed the cluster within a periodically repeated cubic simulation cell and identified its geometrical isomers using first-principles DFT-based electronic structure methods like those described in the previous section. We confirmed the existence of two important groups of isomers which had previously been identified [26,48], the CO-bridging (μ-CO) configurations, Fig. 3a, one of which occurs in the enzyme, and the CO-terminal (CO_T) configurations, Fig. 3b. They differ in the position of one of the CO ligands. In the CO_T isomers, each CO is connected to only one of the two iron atoms, while in μ-CO, as in the enzyme, one of the CO's bridges the two irons, leaving a vacant coordination site V on the distal iron, Fe_d. Within each of the two groups, the isomers differ in the arrangement of the ligands on Fe_p and the ligands plus the vacant coordination site on Fe_d.

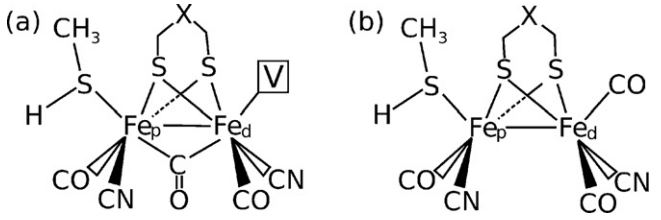

Fig. 3. Model of the $[FeFe]_H$ cluster terminated by $HSCH_3$ in the bridging (a) and terminal (b) configurations. In (a), the configuration in the enzyme, the distal iron has a vacant site, indicated by V, which can coordinate ligands such as CO, H_2O. The "X" in the chelating $S–CH_2–X–CH_2–S$ group stands for CH_2, NH or O [4].

We have simulated H_2-production cycles for the various configurations by adding in sequence two electrons and two protons. Each of these additions proved to be exoenergetic, as did molecular hydrogen desorption. We therefore characterized the catalytic activity of each configuration by the magnitude of the barrier we found for the desorption. The pathways with the most favorable kinetics are those of the μ-CO isomers, which have significantly lower energy barriers than the CO_T configurations. The two successive protonations and subsequent hydrogen desorption occur at the vacant coordination site. The most favorable of these CO-bridging pathways starts from isomers where the distal CN^- ligand is in the *up* position, the vacancy V in the *down* position, and the remaining distal CO is either *cis* or *trans* with respect to the proximal CO, Fig. 3a. These isomers, not observed in the available enzyme X-ray structures, are only marginally less stable than the most stable CO_T isomer, Fig. 3b. The reaction profiles for both cases are shown in Fig. 4 [6]. The energy barrier for the bridging isomer in Fig. 4b is a very promising 1.6 kcal/mol (0.07 eV), whereas that for the terminal isomer in Fig. 4a is a discouraging 12.5 kcal/mol (0.54 eV). The bridging site between the Fe's is open and accessible to protons in the CO_T isomers. The protons bind very strongly there, causing the large barrier.

There are two important design considerations to be gleaned from these results. First, the CO_T configurations are to be avoided by decisively stabilizing a suitable μ-CO configuration. Second, as the cluster is ultimately to be attached to an FeS_2 (1 0 0) surface and immersed in water, the vacancy should be open to the water and accessible to protons, not trapped between the cluster and the surface. This is best achieved with isomers with the distal CN^- ligand in the *down* position and the vacancy V in the *up* position, opposite to their positions in the configurations most favorable in vacuo. While these design considerations could be regarded as firmly established, the quantitative results for such sensitive parameters as the relative energies of the configurations and values of energy barriers could only be taken as indications, as those could well be changed significantly by immersion of the cluster in water and by its attachment to the electrode. Moreover, even qualitative aspects of the pathways could change as electrons and protons are added by hand. Accordingly, the next step towards the development of the electrocatalyst design was to immerse the same cluster in water, providing protons for the reaction in a more realistic way but still adding electrons by hand.

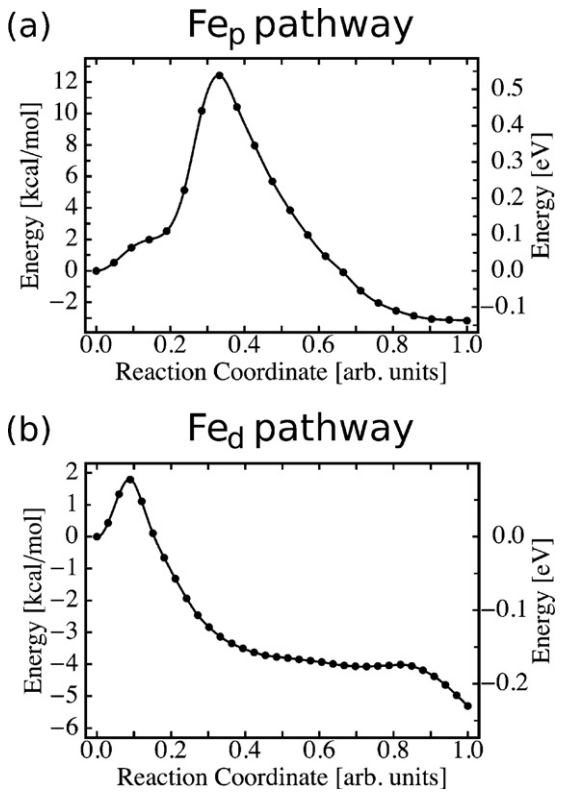

Fig. 4. Energy profiles for desorption of an H_2 molecule from the model $[FeFe]_H$ cluster of Fig. 3 along the two pathways described in the text (Fe_p pathway (a) and Fe_d pathway (b)). The black dots correspond to the energies calculated along the optimized reaction pathway with the NEB method (the minimum energy path). The continuous black line represents a cubic interpolation.

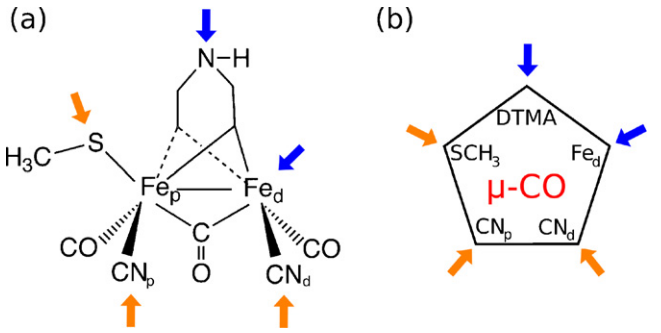

Fig. 5. (a) Model of the $[FeFe]_H$ cluster used in Ref. [7]. The five sites that can be protonated are indicated by arrows. Blue arrows indicate the DTMA and the Fe_d, whose protonation contributes to H_2 production. Orange arrows indicate the other three sites that we have investigated: SCH_3, CN_p, and CN_d. (b) Pentagon diagram used to represent the five sites of the cluster that can be readily protonated; the geometry of the cluster (bridging or terminal) is specified within the pentagon. (For interpretation of the references to color in this figure legend, the reader is referred to the web version of the article.)

4. Water induced changes

To examine how a water environment would effect the composition, structure, and catalytic activity of the naked active site, we placed the $[FeFe]_H$ cluster in a cubic simulation cell and added water [8]. The most detailed simulations were carried out with a cell edge of 14.287 Å and 81 water molecules added to achieve a realistic water density. While electrons were still added by hand during the course of the production cycle, protons added to the water formed hydronium ions and could migrate to the cluster via the Grotthuss shuttle mechanism [49]. Use of FPMD allowed detailed simulation of proton transfer to the cluster. For cluster configurations of particular interest generated during the MD runs, structural optimizations in vacuo were performed for energetic analysis.

The first noteworthy result of these simulations was that at room and somewhat higher temperatures, proton and deprotonation could occur at multiple sites as could isomeric rearrangements, the possible structures numbering in the hundreds. Similarly, there could be a correspondingly large number of pathways for hydrogen production. At issue is the identification of the most probable and relevant structures and pathways. By considering only the most stable among the structures and those of most significance for catalytic activity, we winnowed them down to a manageable number, see Fig. 5 (from Ref. [7]). Examples of structural transitions between different configurations observed during FPMD runs are shown in Fig. 6 (from Ref. [7]).

As expected from the vacuum studies, hydrogen production occurs facilely at the vacant coordination site of Fe_d in the μ-CO configurations. Most interestingly, protonation of the distal CN, $(CN)_d$, to form $(CNH)_d$ results in stabilization of the desired vacancy-up configuration (cf. the comment at the end of Section 3). The first protonation of Fe_d was found to be the rate-limiting step in the production reaction, tagging this as an issue to be addressed when studying the cluster attached to the electrode. Also as expected, H_2 could be formed in the open bridging position of the CO_T configurations, but the activation energy for its desorption would be large, 11 kcal/mol (0.47 eV) for the vacuum case illustrated in Fig. 9 of Ref. [7]. Examination of the total energy distributions of the CO-bridging and CO-terminal configurations observed in water over the course of simulation runs shows that the energy distribution of the most stable CO_T configuration overlaps those of the stables μ-CO configurations, cf. Fig. 12 of Ref. [7]. We found that the bridging region of the CO_T configuration is locally hydrophobic and that protons could not reach it during our simulations. Nevertheless, time spent in that configuration and the dwell time of H_2 on it degrade the catalytic activity of the cluster.

The results of these more realistic water studies emphasize further the importance of locking the cluster into the μ-CO V-up configuration, a conclusion already reached from the vacuum studies, but now with a need to eliminate structural lability and to stabilize the most favorable protonations. The observation that hydrogenation of $(CN)_d$ stabilizes the μ-CO V-up configuration in water is important when considering the cluster attached to the electrode. Two more observations are important as well. First, protonation of the methylthiol weakens its link to Fe_p, raising a serious question as to the stability of a thiol link to the electrode, a link analogous to that within the enzyme. Second, a novel bridging configuration was observed to form spontaneously during one of our simulations. In it the μ-CO is interchanged with the $(CNH)_d$ while maintaining the vacancy in the up position. We designated it as the μ-$(CNH)_d$ configuration. As shown in the next section, this proves key to stable attachment of the cluster to the electrode surface with V-up.

5. Designing an electrocatalyst

5.1. Requirements

To function successfully in the environment defined by the pyrite surface and the acidified water, so different from that within the enzyme, the $[FeFe]_H$ cluster must be modified so as to meet four design requirements

a) The cluster–pyrite linkage must be stable.
b) There must be a vacant coordination site V on Fe_d; V must be exposed to the aqueous environment.

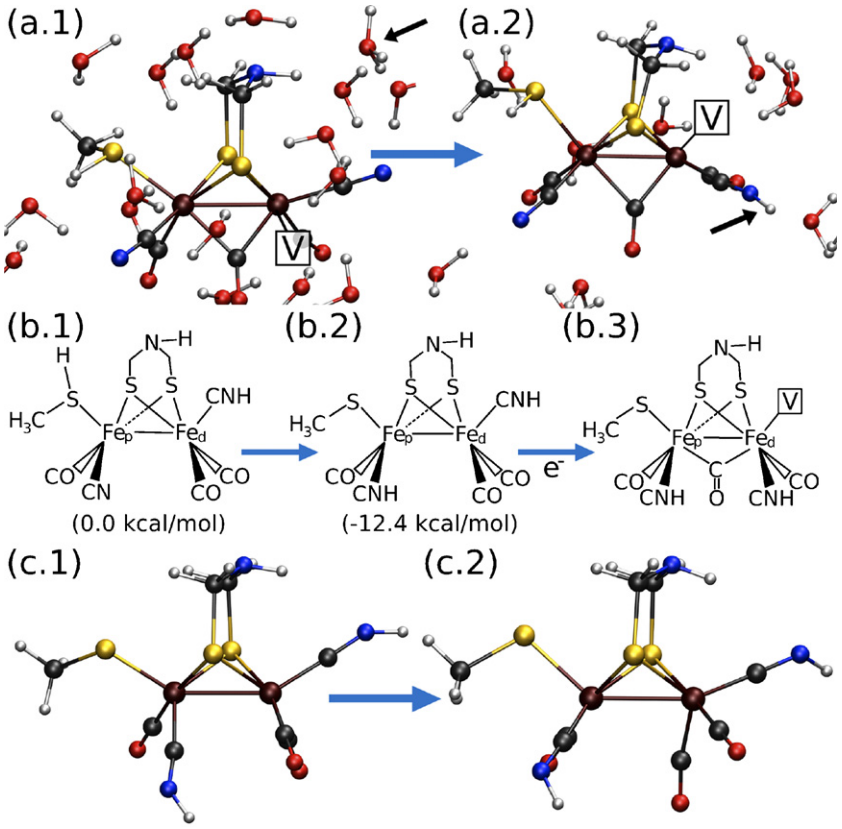

Fig. 6. Transformations (indicated by blue arrows) observed within 1–2 ps during finite-temperature FPMD simulations of the model $[FeFe]_H$ cluster in a water environment. (a.1) The $[FeFe]_H{}^{-1}$ cluster in water containing one hydronium ion (indicated by a black arrow). (a.2) After protonation, CN_d (black arrow) moves "down", while V moves "up". (b.1) The neutral CO_T with CN_d protonated is not stable in water; water molecules abstract the proton from the methyl-thiol and protonate the CN_p. (b.2) The stabilization energy of this proton transfer is 0.54 eV in vacuo. The outcome is a cluster with both CN groups protonated and no proton on the methyl-thiol. (b.3) After adding one electron, the CO_T isomer in water converts to the μ-CO configuration, whereas in vacuo the corresponding transformation from (c.1) is to a semibridging configuration (c.2). The color code is that of Fig. 2. (For interpretation of the references to color in this figure legend, the reader is referred to the web version of the article.)

c) The cluster itself must be stable throughout the H_2 production cycle.
d) The modifications of the cluster needed for requirements (a)–(c) must not interfere with its H_2 production capacity.

5.2. FeS_2 (1 0 0) surface

The stoichiometric (1 0 0) surface of pyrite is formed by breaking the Fe–S bonds between adjacent (1 0 0) atomic layer planes while keeping intact the sulfur-dimer units. The S and Fe atoms on the FeS_2 surface (bulk) are three(four)- and five(six)-fold coordinated, respectively. The LUMO of the clean defect-free surface derives from the d_z^2 orbitals of the surface iron atoms, and the computed band gap is 0.50 eV (0.42 eV for bulk pyrite, compared to the experimental value of ∼0.9 eV [5], a typical DFT underestimate). This inaccuracy, however, is not important in the present context in which the (adiabatic) ground-state electronic structure is always considered

Water adsorption on the FeS_2 (1 0 0) surface has been extensively studied both theoretically [21,24,50–52] and experimentally [53,54]; see Refs. [55,56] and references therein. In agreement with those studies, our calculations show that water adsorbs in molecular form via a coordinative covalent bond between a lone-pair orbital of its oxygen and an empty d_z^2 orbital of a surface iron atom. The computed adsorption energy is 13.1 kcal/mol (0.57 eV) at low (1/8 ML) coverage. Due to intermolecular H-bond formation, this binding energy increases slightly with increasing coverage and becomes 14.3 kcal/mol (0.62 eV) at full (1 ML) coverage. While water adsorbs stably on all exposed Fe sites of the functionalized and bare pyrite (1 0 0) surfaces at $T = 0$ K, full coverage on exposed Fe surface sites is not observed in our finite temperature simulations.

5.3. Stages in the design of the supported catalyst $[FeFe]_P$ [8,9]

Our initial hypothesis for the supported catalyst is sketched in Fig. 7. However, in order to satisfy all four requirements stated in Section 5.1, several modifications of the composition and structure of the cluster are necessary. The conceptual path towards the final form of the catalyst is described in detail in Ref. [8]. In analogy to the link between the $[FeFe]_H$ cluster and the cubane in the enzyme, one could imagine attaching the catalyst to the pyrite surface by using the sulfur atom (S) of an SCH_3 to connect the Fe_p to one of the surface Fe atoms (Fe_{surf1}), as in Fig. 4. However, the finding that protonation of the S atom of the SCH_3 in water weakens the Fe_p-thiol bond which can subsequently break [7] indicates that the link with the electrode should *not* be made with the terminating thiol even though the corresponding link is stable in the enzyme [8]. To overcome this problem we removed the thiol to allow a direct bond between Fe_p and a sulfur atom on the FeS_2 (1 0 0) surface, S_{surf}, cf. Fig. 2. We also protonated the CN groups connected to both Fe_p and Fe_d, $(CN)_p$ and $(CN)_d$, as they are usually protonated in acidified water, thus favoring the V-up configuration [7]. The carbon atom of $(CN)_p$ was also protonated, changing it to the ligand $(CHNH)_p$ on Fe_p. The Fe_p–S_{surf} link restores the four-fold coordination that sulfur atoms have in the pyrite bulk. Fig. 8 shows the evolution of the unexpected μ-$(CNH)_d$ configuration from the CO_T structure. The spontaneous formation of this unusual isomer suggests that its energy is close to those of μ-CO and CO_T. We chose

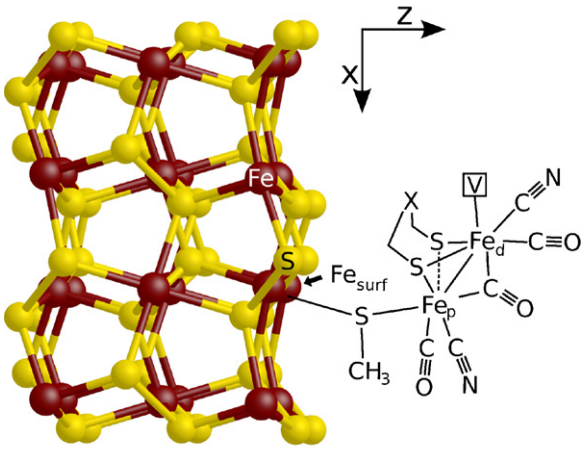

Fig. 7. Sketch of the $[FeFe]_H$ cluster linked to an Fe atom on the FeS_2 (1 0 0) surface. The Fe_4S_4 cubane of the active site of the di-iron hydrogenases (Fig. 1) has been replaced by the pyrite surface, the electrode, and the thiol-cysteine link to the $[FeFe]_H$ cluster has been replaced by an SCH_3, terminating the cluster. The distal iron (Fe_d) has an exposed vacant site, indicated by V, cf. Fig. 3. The pyrite (1 0 0) surface is modeled by a slab nine atomic layers thick. The atoms of the slab are indicated with balls and sticks; the color code is that of Fig. 2. **z** indicates the normal to the surface. (For interpretation of the references to color in this figure legend, the reader is referred to the web version of the article.)

this previously observed isomer for our model catalyst so that a dative bond between the N atom of its μ-$(CNH)_d$ group and a surface iron atom (Fe_{surf1} in Fig. 2) can be used to lock the system into the bridging configuration with the vacant site on Fe_d exposed to H_2O. A third bond with the surface can also form between the N atom of $(CHNH)_p$ and a second iron atom on the surface, Fe_{surf2} in Fig. 2, resulting in a very stable tridentate linkage of the cluster to the electrode.

In the enzyme, the di-iron cluster is bridged by a di-thiol chelating group, DTMA. Replacement of the DTMA bridge by a PDT bridge simplifies the reaction mechanism and therefore its eventual fine tuning. We completed the formation of $[FeFe]_P$ by replacing the S atom of the di-thiol bridge further from the surface, S_{chel}, with a hydrogenated phosphorus, PH, to prevent breakage of the Fe_p–S_{chel} bond upon hydrogenation of S_{chel}, which has a negative impact on the catalytic activity [8]. The ability of the P atom to retain four bonds in this environment opens a further degree of freedom. The H atom connected to the P can be replaced by any organic group R which can be used to tune the properties of the catalyst and the synthetic pathway. Finally, neutral $[FeFe]_P$ linked as described to the pyrite surface and optimized in vacuo is stable with V-up on Fe_d, cf. Fig. 2.

The modified di-iron cluster occupies roughly half of the surface of the simulation cell used here. The surface is thus densely functionalized, cf. Fig. 9. The distance of closest approach between the cluster replicas is 3.35 Å, that between the H atoms of the $(CN)_d$ of one cluster and of the $(CN)_p$ of its neighbor. The use of this simulation cell allows studying H_2 formation at high coverage within an affordable computation time. Of the eight Fe atoms in the surface unit cell shown in Fig. 9, two are linked to the cluster, two though not linked to the cluster are shielded by it from the water, and the remaining four are exposed to the water and bind water molecules as described in Section 5.2.

5.4. H_2 production by $[FeFe]_P$

The changes described above leading from the methylthiol terminated $[FeFe]_H$ cluster to the $[FeFe]_P$ cluster linked to the pyrite surface meet requirements (a) through (c) [8]. The extent to which requirement (d) is met was examined in Ref. [9]. For H_2 production, two electrons and two protons are added sequentially to the catalyst/electrode/water system, the electrons to the catalyst/electrode

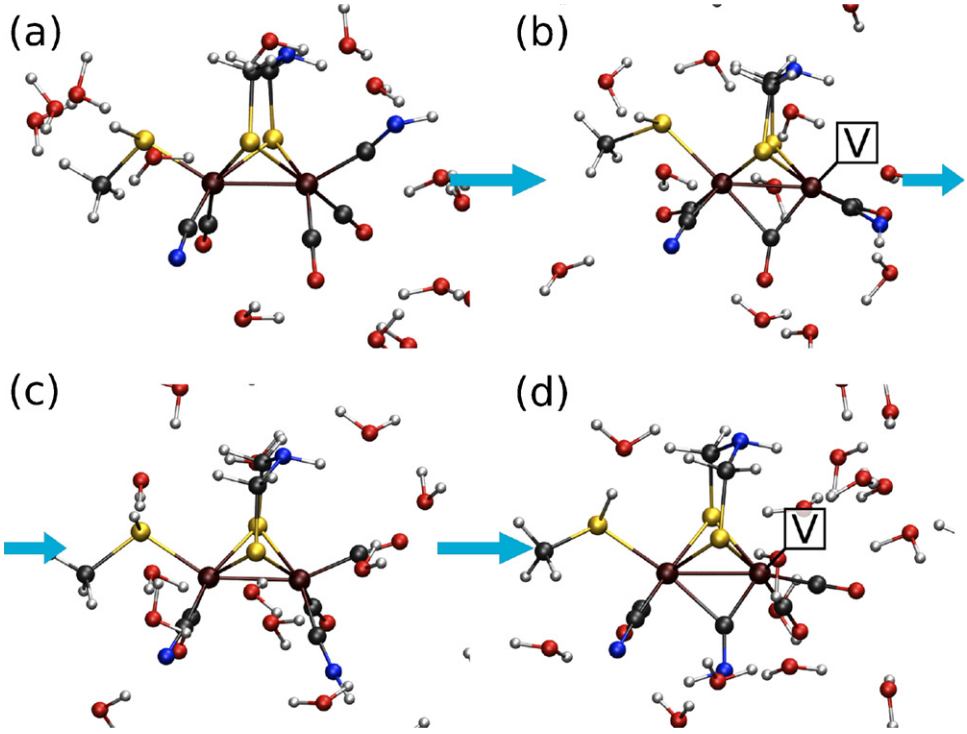

Fig. 8. Snapshots from a FPMD simulation reported in [7] showing the evolution of the negatively (−1) charged CO_T configuration of $[FeFe]_H$ with the CN_d and methyl-thiol groups both protonated (a). This CO_T cluster is not stable in vacuo or in water; at RT it transforms to (b) μ-CO, V-up. At $T = 300$–350 K, the latter doubly-protonated μ-CO is also not kinetically stable, converting into CO_T with CO_d-up, CN_d-down cis (c) in less than 2.0 ps and subsequently to (d), an unusual structure with the protonated CN_d bridging the two Fe-atoms and V-up, obtained dynamically in water only. The color code is that of Fig. 2. (For interpretation of the references to color in this figure legend, the reader is referred to the web version of the article.)

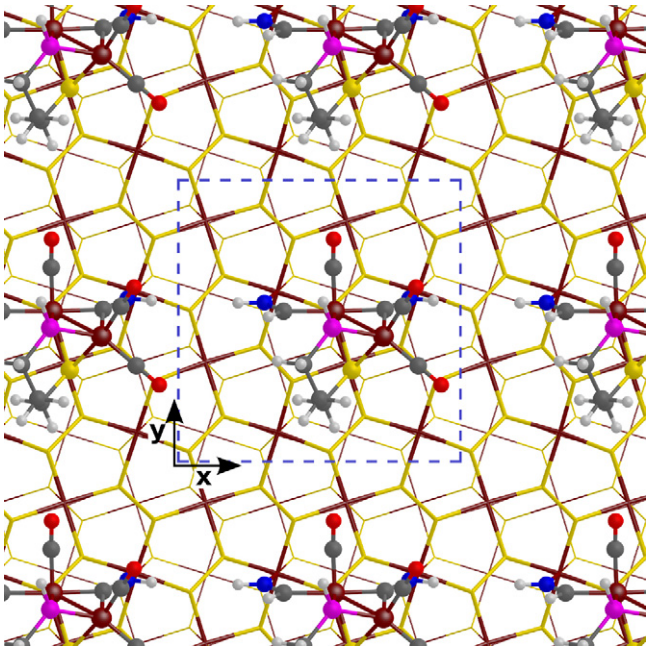

Fig. 9. Top view of the FeS_2 (1 0 0) surface functionalized with the $[FeFe]_P$ cluster of Fig. 2. The geometry has been replicated in the (x, y) plane; the dashed blue line indicates the surface unit cell. The atoms of the cluster are represented with balls and sticks, and the atoms of the slab are represented with sticks only. The color code is that of Fig. 2. (For interpretation of the references to color in this figure legend, the reader is referred to the web version of the article.)

subsystem and the protons to the water. The questions to be answered for each stage of the cycle are: where are the added electrons? What are the proton trajectories, and, in particular, where are the protons added to the cluster? Is there a rate limiting step having a significant free energy barrier? The questions to be answered for the cycle as a whole are: does the linkage of the cluster to the electrode remain stable? Does the structure of the cluster remain stable with V in the exposed up position and the chelating bridge intact?

Before attempting to answer those questions for the cycle in the presence of water, a preliminary investigation was carried out in vacuo. The answers to those questions were positive, and the resulting cycle is illustrated in Fig. 10. The answers are positive for the cycle in water as well. Both the cluster–electrode linkage and the cluster structure remain stable throughout the cycle, which is started with the functionalized electrode in the singly negatively charged state symbolized by $[FeFe]_P^{-1}$. Both proton additions after the electron additions take place entirely at V. The structural and compositional modifications leading to $[FeFe]_P$ eliminate all other protonation sites and all structural lability and greatly simplify the reaction mechanism. The HOMO and LUMO for typical configurations of the system selected from a simulation run are both almost entirely on the slab (90–95%) and delocalized within it for $[FeFe]_P^{-1}$. With the LUMO localized on the electrode, the second electron added to $[FeFe]_P^{-1}$ in the first step of the cycle remains primarily on the electrode, and the formation of a hydrogen atom on Fe_d involves a dynamically coordinated transfer of the proton to V and of an electron from the electrode to the proton (coupled electron–proton transfer). It is this first protonation of the cluster which is the rate-limiting step in the cycle. The addition of one more electron and one more proton results in spontaneous

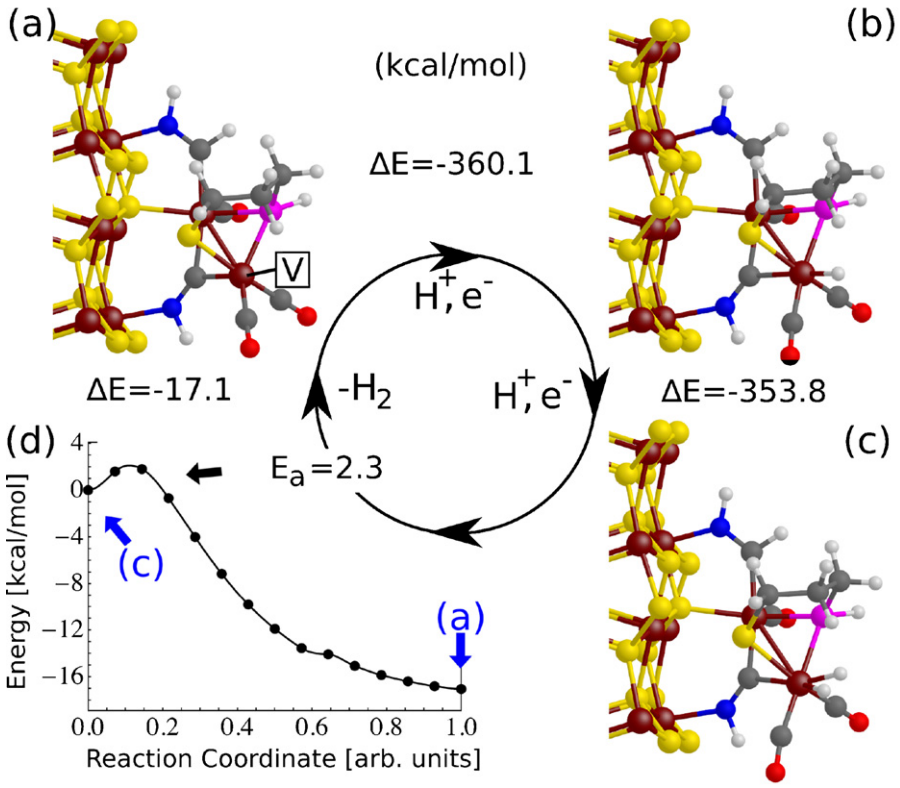

Fig. 10. Catalytic cycle in vacuo for H_2 production by the $[FeFe]_P$ catalyst. (a) Starting configuration with a vacant site on Fe_d; the total charge is −1. (b) The first H atom has been added to Fe_d. (c) The second H atom has been added to Fe_d. ΔE indicates the energy change (in kcal/mol), and (d) E_a is the energy barrier encountered during desorption of a H_2 molecule from (c) to (a) along the minimum-energy path computed via the string method at $T = 0$. The continuous black line represents a cubic interpolation. The color code is that of Fig. 2. (For interpretation of the references to color in this figure legend, the reader is referred to the web version of the article.)

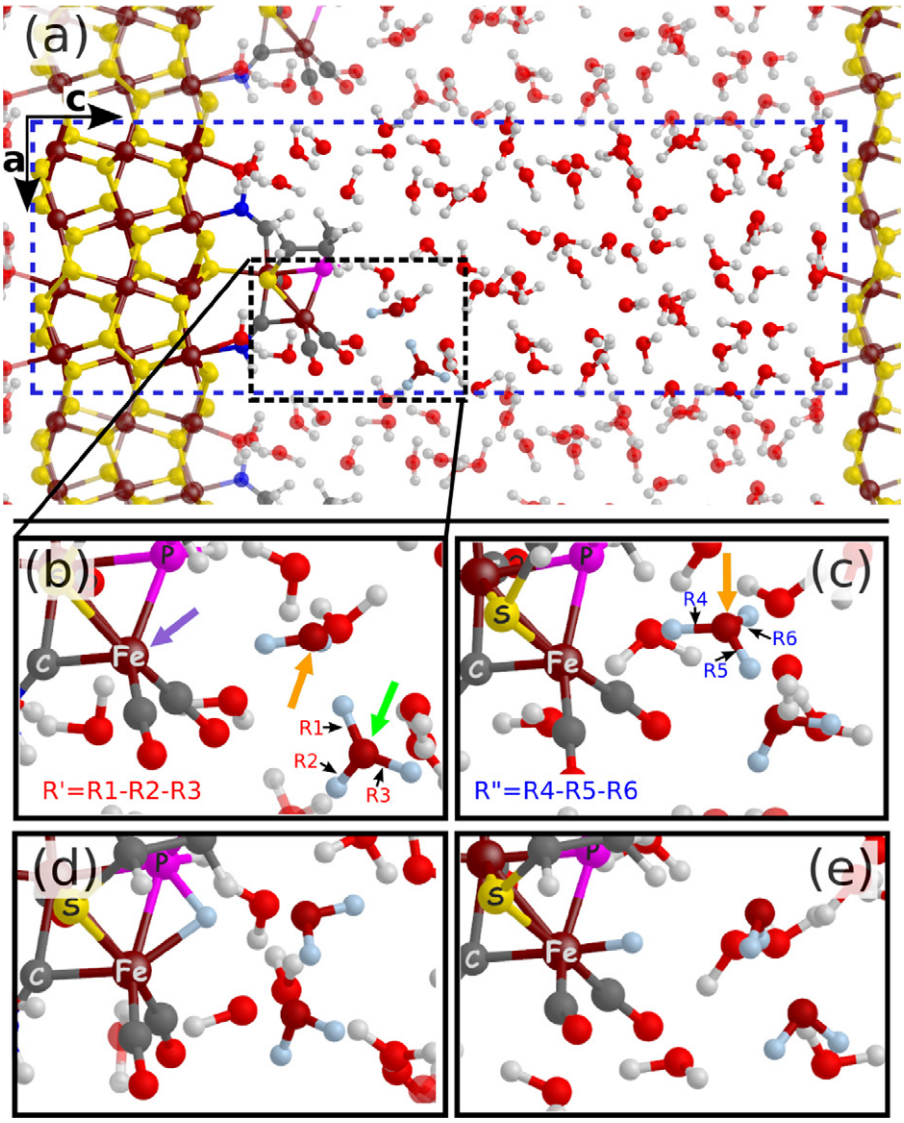

Fig. 11. Protonation of Fe_d in water with an extra proton via constrained FPMD. The total charge of the system is zero. The panels (a)–(e) correspond to snapshots of a constrained FPMD trajectory at $T = 330$ K. (a) Starting configuration with a vacant site on Fe_d and a hydronium ion nearby. The simulation box is bounded by a blue solid line. The O and H atoms involved in the proton transfer are indicated with darker red and light blue balls, respectively. The color code for the remaining atoms is that of Fig. 2. (b) Enlarged view of the reactive region indicated by a dotted box in (a). The purple and the green arrows indicate Fe_d and the hydronium ion. The orange arrow indicates a water molecule bridging the H_3O^+ and Fe_d. $R1$, $R2$, and $R3$ are the O–H bond lengths of the hydronium. $R' = R1 - R2 - R3$ is the reaction coordinate used to transfer one proton from the O-atom indicated with the green arrow to that indicated with the orange arrow. (c) The final configuration obtained varying R' continuously from -1.05 Å to -0.65 Å. $R'' = R4 - R5 - R6$, with $R4$, $R5$, and $R6$ the O–H bond lengths of the hydronium indicated by the orange arrow, is the reaction coordinate for the transfer of the proton to Fe_d. (d) The final configuration with Fe_d–H obtained by varying R'' continuously from -1.03 Å to -0.07 Å starting with the configuration of panel (c). (e) The configuration with Fe_d–H obtained after removing the constraint R'' starting with the configuration of panel (d). (For interpretation of the references to color in this figure legend, the reader is referred to the web version of the article.)

second protonation of Fe_d followed by rapid, spontaneous desorption of an H_2 molecule, returning the system to its starting state.

After the second electron is added to $[FeFe]_P^{-1}$, an added proton moves towards Fe_d by a complex pathway illustrated in Fig. 11 by a series of snapshots taken from a simulation. Because of the existence of a free-energy barrier, the simulation was carried out by constrained FPMD, as described in the figure caption, to prevent the proton from wandering away from the catalyst and not returning in the brief duration of the simulation. Accurate determination of a free-energy barrier by thermodynamic integration [57] for a system of this complexity is computationally very demanding. Limited by what was for us an acceptable computation time, we obtained an upper bound of 8.2 kcal/mol (0.36 eV) for the barrier. The corresponding free-energy profile along the approximate reaction pathway is shown in Fig. 12.

While this barrier is not large for a room temperature reaction, reducing it would be desirable. The barrier could in principle be tuned lower by replacing the H of the PH moiety by a group which modifies the water configuration in the immediate vicinity of Fe_d. The desired configuration would be one in which one of the protons of the nearest water molecule points towards Fe_d, as is the case prior to the second protonation but not prior to the first protonation. Indeed, that relatively close approach of the nearest water proton to the first hydrogen provides both a direct path for the second proton from a hydronium and a favorable initial binding configuration. Carrying out such a design study requires many simulations and therefore a more powerful method of barrier determination would be desirable, as discussed further in the next section.

More generally, in hydrogenation reactions involving electron and proton transfer to the hydrogenation site there is always a

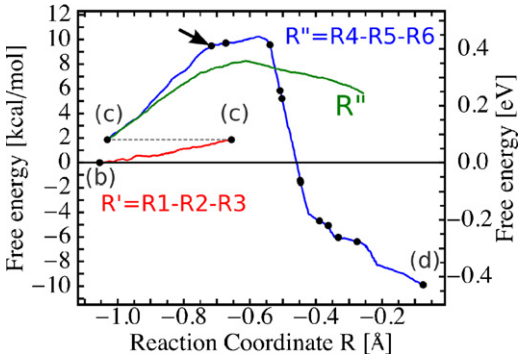

Fig. 12. Free energy profile obtained by thermodynamic integration of the two reaction coordinates R' (red solid line) and R'' (blue and green solid lines). The labels (b)–(d) refers to the geometries of Fig. 11b–d, respectively. The solid red line corresponds to the free energy for transferring a proton from the configuration of Fig. 11b to that of Fig. 11c, using R' as reaction coordinate. The target value of the constraint was changed continuously in a simulation lasting 1.2 ps. The solid blue line shows the free energy for transferring the proton to Fe_d, Fig. 11d, obtained via thermodynamic integration of the reaction coordinates R'' varied continuously from −1.03 Å to −0.07 Å starting with the configuration of Fig. 11c during a simulation lasting 10.7 ps. The black arrow indicates the point at which the speed R'' was changed. The simulation moving the system from (c) to the arrow lasted 1.4 ps, and that moving from the arrow to (d) lasted 9.3 ps. The solid green line shows the free energy for transferring the proton to Fe_d obtained in a simulation lasting 15.4 ps by varying R'' with the speed used in the second part of the simulation associated with the solid blue line. The free-energy barrier to protonation of Fe_d is 8.2 kcal/mol. The gray dotted line indicates the discontinuity due to the change of the reaction coordinate R' to R''. The configurations of Fig. 11b–d are indicated on the profile by the corresponding letters. (For interpretation of the references to color in this figure legend, the reader is referred to the web version of the article.)

question as to which of three possibilities takes place: electron first, proton first, or coordinated transfers of both? In our case, the third possibility occurs, dynamically coordinated transfer of the electron from the FeS_2 electrode and of the proton from a hydronium to Fe_d. This differs from what happens in the enzyme, where the active state of the cluster is $[FeFe]_H{}^{-1}$, i.e. FeIIFeI, ready to receive a proton with the electron already transferred from the Fe_4S_4 cubane [43].

6. Limitations and mitigations

As in all first-principles simulations of complex systems, to bring the computational load down to manageable size choices were made with regard to computational methods and system size which introduced limitations to the accuracy of the results. In this section, we identify the most significant of these limitations, outline steps that can be taken to mitigate those limitations, and report some preliminary progress.

The key elements of the catalytic mechanism are two successive electron transfers from the electrode to the cluster interwoven with two successive proton transfers from the water to the cluster. Each formation of an H atom at Fe_d proceeds by dynamical coordination of the motions of the electron and the proton transfers during the formation and binding of the H atoms. This process is sensitive to the details of the electron charge distribution over the cluster and the electrode and in particular to the degree of localization of the most important Kohn–Sham electronic states [58], notably the HOMO and LUMO of the system. Their localization affects, for example, the electron-transfer matrix elements between the electrode and Fe_d and the electrostatic field in the water near the cluster, which in turn affects the proton shuttle.

The *geometric* parameter to which the degree of localization is most sensitive is the thickness of the FeS_2 slab. Our computations were all performed with a slab containing 9 atomic layers. To test the dependence of localization and the details of where the added electrons go at each stage of the cycle, we repeated key computations for a slab 21 layers thick. That major thickness change caused a minor increase in the localization of the added electron charge on the electrode, with less going to the cluster. When the electron is transferred from the electrode to the proton on protonation, a correspondingly larger fraction comes from the electrode and less from the cluster atoms. The changes in atomic charges within the cluster are delocalized. A particularly important effect of increasing slab thickness is a much increased degree of localization of the HOMO *within* the slab to its top surface for $[FeFe]_P{}^{-1}$, which would enhance the electrostatic field attracting the proton and could decrease the activation free energy for first protonation, the rate limiting step in H_2 formation.

The choice of density functional is also very important for localization. We used a semi-local, gradient-corrected density functional, PBE [11]. One of the limitations of all local and semi-local functionals is that they include some self interaction, which causes the Kohn–Sham orbitals to spread out in compensation. That is, they tend to delocalize the electron states. This effect may be particularly important for the Fe atoms central to the chemistry because of their high local electron density. Hybrid density functionals, such as PBE0 [59], compensate for the self interaction in PBE by mixing in a fixed amount of the exact exchange functional, based on general considerations, with good results (e.g. Ref. [60]). Thus use of PBE0 would be interesting, but calculating exact exchange for systems as complex as the present would be very expensive computationally. Our group has recently developed a method for V_{ex} which scales linearly with system size and which should allow, in principle, performance of such a calculation [61]. Another, more affordable approach would be use of the LDA + U method [62–64] which is limited to effects associated with d-orbitals, whereas PBE0 treats all orbitals on the same footing. At issue throughout is how correctly increasing localization affects the barrier to first protonation.

The thickness of the water layer is a geometric parameter of importance to the magnitude of the electrostatic field experienced by a proton near the cluster when the decorated electrode is charged. We have confirmed that increasing the vacuum space between adjacent repeated slabs before inserting the water molecules significantly increases the electric field immediately above the cluster, a very simple consequence of the classical electrostatics of charged slabs. This increase in field would be substantially reduced by the dielectric screening of water; its expected effect would be to reduce the barrier to first protonation and enhance proton transfer generally.

As mentioned in Section 5.4, we have obtained an upper limit of 8.2 kcal/mol (0.36 eV) for the free-energy barrier to the first protonation using what is a current state of the art thermodynamic-integration method. To obtain a value rather than a bound, a faster method is needed, one which allows use of a multidimensional reaction coordinate and is more readily parallelized. Such a method is prerequisite to the fine tuning of the reaction kinetics of the first protonation allowed for by the substitution of suitable groups for the H of the PH group of $[FeFe]_P$. A search for a suitable method is in progress.

Another limitation is that proton motion is treated classically in FPMD. Quantum effects enter in two different ways. The first is that the minimum energy a proton has in moving in the vicinity of a local minimum in the potential energy surface is above the value of the minimum by its zero-point energy, which is larger than its classical thermal energy 3 kT. The mean kinetic energy of a proton in liquid water at 23 °C is 3.4 kcal/mol (147 meV [65], compared to the classical kinetic energy 3/2 kT, 0.78 kcal/mol). The associated potential energy would be the same for purely harmonic motion above the minimum. This could have the effect of reducing the activation energy for the first proton transfer by an amount on the same scale as our calculated upper bound of 8.3 kcal/mol for the

activation free energy. The second is quantum tunneling which, when translated into classical terms, also has the effect of barrier reduction.

Another issue inadequately addressed is the relation between our simulations and the real world of electrochemistry. Of particular importance would be determining the electrode potential at each stage of the hydrogen production cycle. This is not trivial within the periodic boundary conditions adopted for our calculations.

In sum, the preliminary studies of limitations and their mitigation we have done thus far suggest that the kinetics of first protonation could be more favorable than indicated by the published computations we have reviewed in Sections 3–5, Refs. [6–9].

7. Discussion and conclusions

The work we have reviewed here has an explicit goal, the theoretical design of a potentially useful electrocatalyst for hydrogen production, and an implicit goal, the demonstration that it is feasible to use first-principles molecular-dynamics computations in the theoretical design of systems as complex as that studied here consisting of an electrode with an attached catalyst in the form of a cluster of nontrivial size immersed in a liquid. There have been in recent years several other *ab initio* studies of electrocatalytic reactions at solid–liquid interfaces, mainly on metals [66,67], but also metal oxides [68] and especially for hydrogen oxidation/evolution and oxygen reduction. In most cases, however, the modeling of the liquid is simplified, often as just a few layers with little equilibration or as a continuum model. An important lesson to draw from our work is that it is computationally feasible to treat the electrons of thicker liquid layers in full quantum-mechanical detail.

We have shown within the accuracy of our model and our methods that the $[FeFe]_P$ cluster binds stably to the FeS_2 (100) surface and retains the critical V-up configuration throughout the hydrogen-production cycle. We have found that the rate-limiting step in the production reaction is the first protonation, $[FeFe]_P^{-1} + H^+ \rightarrow H[FeFe]_P$, with an upper bound to its free-energy barrier of 8.2 kcal/mol (0.36 eV), implying that the functionalized electrode would be a good catalyst. We have good reason to believe that computations improved as discussed in Section 6 and the neglected quantum effects would yield a barrier significantly below that figure. Nevertheless, while promising progress has been made, problems remain. In particular, electrocatalytic hydrogen production would necessarily occur in a half cell during the full electro- or photoelectro-catalysis of water, with oxygen generated in the other half cell. How to protect the catalyst and any exposed FeS_2 surface from oxygen attack is a design issue not yet addressed. To do so and to address also the problem of the electrode potential, it might be useful to introduce QM/MM or better FPMD combined with MM, as it would allow modeling of a much larger system comprising several thousands of molecules of water in the MM part. The challenge then would be to render innocuous the transition-region errors, as raised in Section 1.

What has been clearly demonstrated is the potential of FPMD for chemical design for heterogeneous catalysis in which the catalyzed reaction takes place at an interface between a solid and a liquid. FPMD allows accurate description of the atomic dynamics within the liquid, of the quantum mechanics of electron redistribution, of how that redistribution affects the dynamics within the liquid, and of atomic and molecular transfers to or from the catalyst or the liquid coordinated with electron redistribution as the case may be. The detailed insight it thereby provides was essential to the design process we summarized in Section 5. For example, the replacement of S_{chel} by PH was informed by the insight that the Fe_p–S_{chel} bond had been weakened by the stronger, diametrically opposed Fe_p–S_{surf} bond to the point that it would break upon the protonation of S_{chel} since sulfur cannot sustain 4 strong bonds. This indicated that S_{chel} had to be replaced by an atom which could sustain 4 strong bonds yet was small enough not to compress the space of the vacant coordination site V on Fe_d. Only a group PR, with R covalently linked to P and not encroaching upon V would meet these requirements. The simplest R, though not necessarily the optimal one, is H. We anticipate that continued use of FPMD to tune the catalyst by varying R and to explore protection against oxygen will significantly advance the design of a potentially useful electrocatalyst for hydrogen production.

Acknowledgments

This work was supported by the Department of Energy, Office of Basic Energy Sciences, Division of Materials Sciences and Engineering under Award DE-FG02-06ER-46344. This research used resources of the National Energy Research Scientific Computing Center, which is supported by the Office of Science of the U.S. Department of Energy under Contract No. DE-AC02-05CH11231. The simulations presented in this article were in part performed on computational resources supported by the PICSciE-OIT High Performance Computing Center and Visualization Laboratory. Informative and helpful discussions with Andrew B. Bocarsly, G. Charles Dismukes, and Jeffrey Schwartz are gratefully acknowledged.

References

[1] M. Frey, Chembiochem 3 (2002) 153.
[2] S.C. Barton, J. Gallaway, P. Atanassov, Chem. Rev. 104 (2004) 4867.
[3] Y. Nicolet, C. Piras, P. Legrand, C.E. Hatchikian, J.C. Fontecilla-Camps, Struct. Fold. Des. 7 (1999) 13.
[4] Y. Nicolet, A.L. de Lacey, X. Vernede, V.M. Fernandez, E.C. Hatchikian, J.C. Fontecilla-Camps, J. Am. Chem. Soc. 123 (2001) 1596.
[5] I.J. Ferrer, D.M. Nevskaia, C. Delasheras, C. Sánchez, Solid State Commun. 74 (1990) 913.
[6] C. Sbraccia, F. Zipoli, R. Car, M.H. Cohen, G.C. Dismukes, A. Selloni, J. Phys. Chem. B 112 (2008) 13381.
[7] F. Zipoli, R. Car, M.H. Cohen, A. Selloni, J. Phys. Chem. B 113 (2009) 13096.
[8] F. Zipoli, R. Car, M.H. Cohen, A. Selloni, J. Chem. Theory Comput. 6 (2010) 3490.
[9] F. Zipoli, R. Car, M.H. Cohen, A. Selloni, J. Am. Chem. Soc. 132 (2010) 8593.
[10] R. Car, M. Parrinello, Phys. Rev. Lett. 55 (1985) 2471.
[11] J.P. Perdew, K. Burke, M. Ernzerhof, Phys. Rev. Lett. 78 (1997) 1396.
[12] P. Giannozzi, S. Baroni, N. Bonini, M. Calandra, R. Car, C. Cavazzoni, D. Ceresoli, G.L. Chiarotti, M. Cococcioni, I. Dabo, A. Dal Corso, S. de Gironcoli, S. Fabris, G. Fratesi, R. Gebauer, U. Gerstmann, C. Gougoussis, A. Kokalj, M. Lazzeri, L. Martin-Samos, N. Marzari, F. Mauri, R. Mazzarello, S. Paolini, A. Pasquarello, L. Paulatto, C. Sbraccia, S. Scandolo, G. Sclauzero, A.P. Seitsonen, A. Smogunov, P. Umari, R.M. Wentzcovitch, J. Phys. Condens. Matter 21 (2009) 395502.
[13] D. Vanderbilt, Phys. Rev. B 41 (1990) 7892.
[14] K. Laasonen, A. Pasquarello, R. Car, C. Lee, D. Vanderblit, Phys. Rev. B 47 (1993) 10142.
[15] S.L. Finklea, L. Cathey, E.L. Amma, Acta Crystallogr. A 32 (1976) 529.
[16] G.J. Martyna, M.L. Klein, M. Tuckerman, J. Chem. Phys. 97 (1992) 2635.
[17] S. Nosé, Prog. Theor. Phys. Suppl. (1991) 1.
[18] P.E. Blöchl, M. Parrinello, Phys. Rev. B 45 (1992) 9413.
[19] G. Henkelman, B.P. Uberuaga, H. Jónsson, J. Chem. Phys. 113 (2000) 9901.
[20] W.N.E.W.Q. Ren, E. Vanden-Eijnden, Phys. Rev. B 66 (2002) 052301.
[21] N.N. Nair, E. Schreiner, D. Marx, J. Am. Chem. Soc. 128 (2006) 13815.
[22] A. Stirling, M. Bernasconi, M. Parrinello, Phys. Rev. B 75 (2007) 165406.
[23] A. Stirling, M. Bernasconi, M. Parrinello, J. Chem. Phys. 119 (2003) 4934.
[24] A. Stirling, M. Bernasconi, M. Parrinello, J. Chem. Phys. 118 (2003) 8917.
[25] M. Bruschi, C. Greco, M. Kaukonen, P. Fantucci, U. Ryde, L. De Gioia, Angew. Chem. Int. Ed. 48 (2009) 3503.
[26] Z.X. Cao, M.B. Hall, J. Am. Chem. Soc. 123 (2001) 3734.
[27] Z.P. Liu, P. Hu, J. Am. Chem. Soc. 124 (2002) 5175.
[28] M. Bruschi, P. Fantucci, L. De Gioia, Inorg. Chem. 41 (2002) 1421.
[29] C. Greco, M. Bruschi, L. De Gioia, U. Ryde, Inorg. Chem. 46 (2007) 5911.
[30] A.T. Fiedler, T.C. Brunold, Inorg. Chem. 44 (2005) 9322.
[31] S. Zilberman, E.I. Stiefel, M.H. Cohen, R. Car, J. Phys. Chem. B 110 (2006) 7049.
[32] R.K. Szilagyi, M.A. Winslow, J. Comput. Chem. 27 (2006) 1385.
[33] T.B. Liu, B. Li, M.L. Singleton, M.B. Hall, M.Y. Darensbourg, J. Am. Chem. Soc. 131 (2009) 8296.
[34] P.E.M. Siegbahn, J.W. Tye, M.B. Hall, Chem. Rev. 107 (2007) 4414.
[35] J.W. Tye, M.B. Hall, M.Y. Darensbourg, Proc. Natl. Acad. Sci. U.S.A. 102 (2005) 16911.

[36] C. Tard, X.M. Liu, S.K. Ibrahim, M. Bruschi, L. De Gioia, S.C. Davies, X. Yang, L.S. Wang, G. Sawers, C.J. Pickett, Nature 433 (2005) 610.
[37] J.W. Peters, W.N. Lanzilotta, B.J. Lemon, L.C. Seefeldt, Science 282 (1998) 1853.
[38] K.A. Vincent, J.A. Cracknell, O. Lenz, I. Zebger, B. Friedrich, F.A. Armstrong, Proc. Natl. Acad. Sci. U.S.A. 102 (2005) 16951.
[39] W. Lubitz, E. Reijerse, M. van Gastel, Chem. Rev. 107 (2007) 4331.
[40] G.A.N. Felton, A.K. Vannucci, J.Z. Chen, L.T. Lockett, N. Okumura, B.J. Petro, U.I. Zakai, D.H. Evans, R.S. Glass, D.L. Lichtenberger, J. Am. Chem. Soc. 129 (2007) 12521.
[41] M. Hambourger, M. Gervaldo, D. Svedruzic, P.W. King, D. Gust, M. Ghirardi, A.L. Moore, T.A. Moore, J. Am. Chem. Soc. 130 (2008) 2015.
[42] C.E. Lubner, R. Grimme, D.A. Bryant, J.H. Golbeck, Biochemistry 49 (2010) 404.
[43] J.C. Fontecilla-Camps, A. Volbeda, C. Cavazza, Y. Nicolet, Chem. Rev. 107 (2007) 4273.
[44] H.J. Fan, M.B. Hall, J. Am. Chem. Soc. 123 (2001) 3828.
[45] J.A. Cracknell, K.A. Vincent, F.A. Armstrong, Chem. Rev. 108 (2008) 2439.
[46] K.A. Vincent, A. Parkin, F.A. Armstrong, Chem. Rev. 107 (2007) 4366.
[47] A. Silakov, E.J. Reijerse, S.P.J. Albracht, E.C. Hatchikian, W. Lubitz, J. Am. Chem. Soc. 129 (2007) 11447.
[48] Z.P. Liu, P. Hu, J. Chem. Phys. 117 (2002) 8177.
[49] D. Marx, M.E. Tuckerman, J. Hutter, M. Parrinello, Nature 397 (1999) 601.
[50] E. Schreiner, N.N. Nair, D. Marx, J. Am. Chem. Soc. 130 (2008) 2768.
[51] C. Boehme, D. Marx, J. Am. Chem. Soc. 125 (2003) 13362.
[52] J.A. Rodriguez, I.A. Abreu, J. Phys. Chem. B 109 (2005) 2754.
[53] T. Kendelewicz, C.S. Doyle, B.C. Bostick, G.E. Brown, Surf. Sci. 558 (2004) 80.
[54] K.M. Rosso, U. Becker, M.F. Hochella, Am. Mineral. 84 (1999) 1549.
[55] D. Rickard, G.W. Luther, Chem. Rev. 107 (2007) 514.
[56] R. Murphy, D.R. Strongin, Surf. Sci. Rep. 64 (2009) 1.
[57] J.G. Kirkwood, J. Chem. Phys. 3 (1935) 300.
[58] W. Kohn, L.J. Sham, Phys. Rev. 140 (1965) 1133.
[59] J.P. Perdew, M. Ernzerhof, K. Burke, J. Chem. Phys. 105 (1996) 9982.
[60] X.F. Wu, E.J. Walter, A.M. Rappe, R. Car, A. Selloni, Phys. Rev. B 80 (2009) 115201.
[61] X.F. Wu, A. Selloni, R. Car, Phys. Rev. B 79 (2009) 085102.
[62] V.I. Anisimov, J. Zaanen, O.K. Andersen, Phys. Rev. B 44 (1991) 943.
[63] V.I. Anisimov, I.V. Solovyev, M.A. Korotin, M.T. Czyzyk, G.A. Sawatzky, Phys. Rev. B 48 (1993) 16929.
[64] I.V. Solovyev, P.H. Dederichs, V.I. Anisimov, Phys. Rev. B 50 (1994) 16861.
[65] G.F. Reiter, J.C. Li, J. Mayers, P. Platzman, F. Stillinger, Braz. J. Phys. 34 (2004) 142.
[66] M. Otani, I. Hamada, O. Sugino, Y. Morikawa, Y. Okamoto, T. Ikeshoji, J. Phys. Soc. Jpn. 77 (2008).
[67] J.S. Filhol, M. Neurock, Angew. Chem. Int. Ed. 45 (2006) 402.
[68] J. Rossmeisl, A. Logadottir, J.K. Norskov, Chem. Phys. 319 (2005) 178.